Characterizing the Strong Earth Gravity Prior

Björn Jörges[1] and Joan López-Moliner[2]*

1 Center for Vision Research, York University, 4700 Keele Street, Toronto, ON M3J 1P3, Canada

2 Vision and Control of Action (VISCA) group, Department of Cognition, Development and Psychology of Education, Institut de Neurociències, Universitat de Barcelona, Ps. Vall d'Hebron 171, 08035 Barcelona, Catalonia, Spain.

* Corresponding Author

Abstract

Humans expect downwards moving objects to accelerate and upwards moving objects to decelerate. These results have been interpreted as humans maintaining an internal model of gravity. We have previously suggested an interpretation of these results within a Bayesian framework of perception: earth gravity could be represented as a Strong Prior that overrules noisy sensory information (Likelihood) and therefore attracts the final percept (Posterior) very strongly. Based on this framework, we use published data from a timing task involving gravitational motion to determine the mean and the standard deviation of the Strong Earth Gravity Prior. To get its mean, we refine a model of mean timing errors we proposed in a previous paper (Björn Jörges & López-Moliner, 2019), while expands the range of conditions under which it yields adequate predictions of performance. This underscores our previous conclusion that the gravity prior is likely to be very close to 9.81 m/s². To obtain the standard deviation, we identify different sources of sensory and motor variability reflected in timing errors. We then model timing responses based on quantitative assumptions about these sensory and motor errors for a range of standard deviations of the earth gravity prior, and find that a standard deviation of around 2 m/s² makes for the best fit. This value is likely to represent an upper bound, as there are strong theoretical reasons along with support empirical evidence for the standard deviation of the earth gravity being lower than this value.

Introduction

There is ample evidence that humans represent earth gravity and use it for a variety of tasks such as interception (Ceccarelli et al., 2018; La Scaleia, Zago, Moscatelli, Lacquaniti, & Viviani, 2014; McIntyre, Zago, & Berthoz, 2001; Senot et al., 2012; Zago, McIntyre, Senot, & Lacquaniti, 2008), time estimation (Moscatelli & Lacquaniti, 2011), the perception of biological motion (Maffei et al., 2015) and many more. Recently, we have shown that gravity-based prediction for motion during an occlusion matched performance under a 1g expectation not only qualitatively, but also quantitatively (Björn Jörges & López-Moliner, 2019). This was an important finding to support our interpretation of the above results as a strong prior in a Bayesian framework of perception (Björn Jörges & López-Moliner, 2017). The results presented in (Björn Jörges & López-Moliner, 2019) indicate that the mean of this strong gravity prior is roughly at 1g (9.81 m/s²) when the occlusion is long enough. In the present paper, we extend the simulations brought forward in our previous paper: First, we consider how accounting for the Aubert-Fleischl effect, which leads humans to perceive moving object at about 80 % of their actual speed when they pursue the target with their eyes (Aubert, 1887; Dichgans, Wist, Diener, & Brandt, 1975; Fleischl,

1882), can extend our simple 1g-based model to shorter occlusions. Furthermore, to fully characterize a prior, we need to not only indicate its mode, but also its standard deviation. The second goal of the present paper is thus to determine the standard deviation of the strong gravity prior. We aim to achieve this goal by simulations based on assumptions about the different sources of noise relevant to the task at hand.

On a theoretical level, we envision (visual) perception as a two-step process: Encoding and Decoding. During Encoding, low level signals such as luminosity, retinal velocities or orientation are picked up by the perceptual system. However, these low-level sensory signals are ambiguous with respect to the state of the world: for example, the same retinal velocities can correspond to vastly different physical velocities, depending on the distance between observer and object. Decoding, then, is the process of interpreting optic flow information. In Decoding, humans often combine sensory input with previous knowledge to obtain a more accurate and precise estimate of the observed state of the world. For example, we use knowledge about the size of an object to recover its most likely distance to the observer, thus providing a key to recover its physical velocity from retinal motion. In some, if not many instances, this combination occurs according to Bayes' formula:

$$P(A|B) = \frac{P(B|A)P(A)}{P(B)} \qquad [1]$$

The probability of a state of the world A given evidence B is the probability of observing evidence B given the state of the world A multiplied by the probability of the state of the world (A), divided by the probability of the evidence (B). In a Bayesian framework, sensory input (Likelihood) and prior knowledge (Prior) are combined according to their respective precisions to yield a more precise and more accurate final percept (Posterior). Usually both the Prior and the Likelihood contribute to the Posterior; for example when we know that our opponent in a tennis match *usually* serves in the right corner of the court, but *not always*, (Prior) and we have good visibility of their serving motion, but since the motion is so quick, we do not have a lot of time to acquire evidence (Likelihood). We thus take sensory input (e. g. about their body posture while serving) into account only to some extent (see "Normal Prior" scenario in Figure 1). However, in the case of gravity it seems that the expectation of Earth Gravity overrules all sensory information that humans collect on the law of motion of an observed object. On a theoretical level, this is a sensible assumption, since all of human evolution and each human's individual development occurred under Earth Gravity. In Bayesian terms, the Prior is extremely precise and thus overrules all sensory

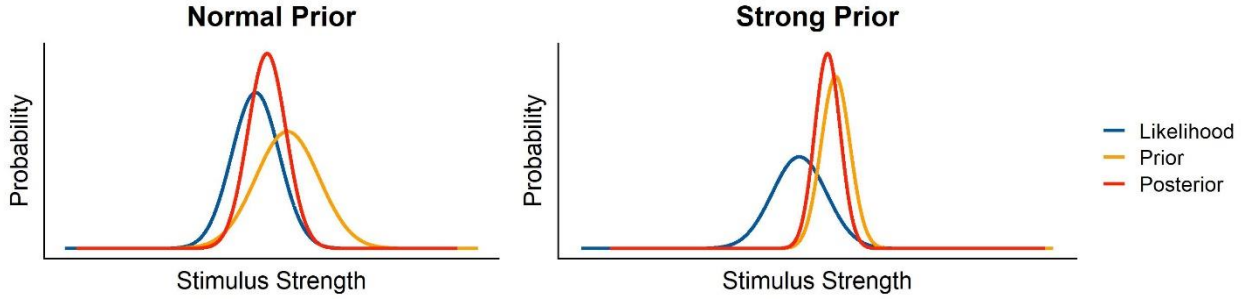

Figure 1: Graphical illustration of Likelihood, Prior and Posterior in a Bayesian framework, for both a normal, relatively shallow Prior, and a strong, extremely precise Prior.

information represented as the Likelihood. According to our interpretation, we would thus expect an extremely low value for the standard deviation of the earth gravity prior.

In the following, we use the data from our previous study (Björn Jörges & López-Moliner, 2019) to simulate the variability of responses under different assumptions about the standard deviation of the gravity prior.

Methods

Participants

A total of ten (n = 10) participants performed the task, among which one of the authors (BJ). All had normal or corrected-to-normal vision. The remaining participants were in an age range of 23 and 34 years, of which five (n = 5) self-identified as women and five (n = 5) self-identified as men. All participants gave their informed consent. The research in this study was part of an ongoing research program that has been approved by the local ethics committee of the University of Barcelona. The experiment was conducted in accordance with the Code of Ethics of the World Medical Association (Declaration of Helsinki).

Stimuli

We presented participants with targets of tennis ball size (radius = 0.033 m), shape and texture that moved on parabolic trajectories. The trajectories were determined by the gravity levels (0.7, 0.85, 1, 1.15, 1.3g, -1g), the initial vertical velocities (4.5 and 6 m/s) and the initial horizontal velocities (3 and 4 m/s). The different kinetic profiles, as well as the occlusion condition (Short Occlusion: last 20-25%; Long Occlusion: last 45-50% of the trajectory), were presented in random order, but the method guaranteed that each combination was presented the same amount of times. The parabolas were presented in the fronto-parallel plane with no change in depth. Air resistance was simulated to provide a more realistic stimulus. The following equations (http://www.demonstrations.wolfram.com/ProjectileWithAirDrag/) determine the x position of the target in time *x(t)*, and the y position of the target in time *y(t)*, respectively, including air resistance:

$$x(t) = \frac{\left({v_{xi}}^2 + {v_{yi}}^2\right)^{0.5} * m * g}{g * c} * \cos\left(\operatorname{asin}\left(\frac{v_{yi}}{\left({v_{xi}}^2 + {v_{yi}}^2\right)^{0.5}}\right)\right) * \left(1 - e^{\left(-\frac{g*t*c}{m*g}\right)}\right) \quad [2]$$

$$y(t) = \left(\frac{m}{c}\right) * \left(\left({v_{xi}}^2 + {v_{yi}}^2\right)^{0.5} * \sin\left(\operatorname{asin}\left(\frac{v_{yi}}{\left({v_{xi}}^2 + {v_{yi}}^2\right)^{0.5}}\right)\right) + \frac{m * g}{c}\right) * \left(1 - e^{\left(-\frac{g*t*c}{m*g}\right)}\right) - \frac{m * g * t}{c} \quad [3]$$

With v_{xi} being the initial horizontal velocity, v_{yi} the initial vertical velocity, *m* the mass of the target (0.057 kg), *g* the respective gravity value and *c* being the drag coefficient, where we chose 0.005.

For description of the parabolas, we use a coordinate system where the observer's position is defined as x = y = z = 0; the x axis runs from left to right, the y axis from down to up and the z axis away from the observer in depth. The starting y position was half a meter above the ground (y = 0.5 m) for positive gravity values (0.7-1.3g) and 3.5 m for negative gravity values (-1g), while the starting x position was moved to the left from the middle of the scene by half of the overall length of the trajectory (x = -length/2 m). The target travels to the right, such that the peak of the parabola was always reached at x = 0 m (or the lowest point for the inverted parabolas). The ball's z position remained constant at z = -6.15 m. The target disappeared at a random point between 20% and 25% (Short Occlusion) or 45% and 50% (Long Occlusion)

of the time it would take for it to return to the initial height (y = 0.5 m or y = 3.5 m, respectively). The y end position was marked with an elongated table that was displayed in the target area of the room for targets with positive gravities; it was marked with an elongated lamp hanging from the ceiling for inverted stimuli. We presented the trajectories in a rich environment that provided 3D cues about the object's position in depth (see Figure 1) and used a known object (a tennis ball) as target to recruit prior knowledge consistent with the geometry on display. This has been shown to help activate the internal model of gravity (Lacquaniti et al., 2013; Monache, Lacquaniti, & Bosco, 2019; Zago, La Scaleia, Miller, & Lacquaniti, 2011), that we have previously suggested to be an earth gravity prior (Björn Jörges & López-Moliner, 2017). This environment was constructed such that no low-level cues such as differences in brightness and contrast with the target differed significantly between the different trajectories.

Apparatus

Two Sony laser projectors (VPL-FHZ57) were used to provide overlaid images on a back-projection screen (244 cm height and 184 cm width) with a resolution of 1920x1080 pixels. The frequency of refresh of the image was 85 Hz for each eye. Circular polarizing filters were used to provide stereoscopic images. Participants stood at 2 m distance centrally in front of the screen and used polarized glasses to achieve stereoscopic vision of the visual scene and the target. The shown disparity was adapted to each

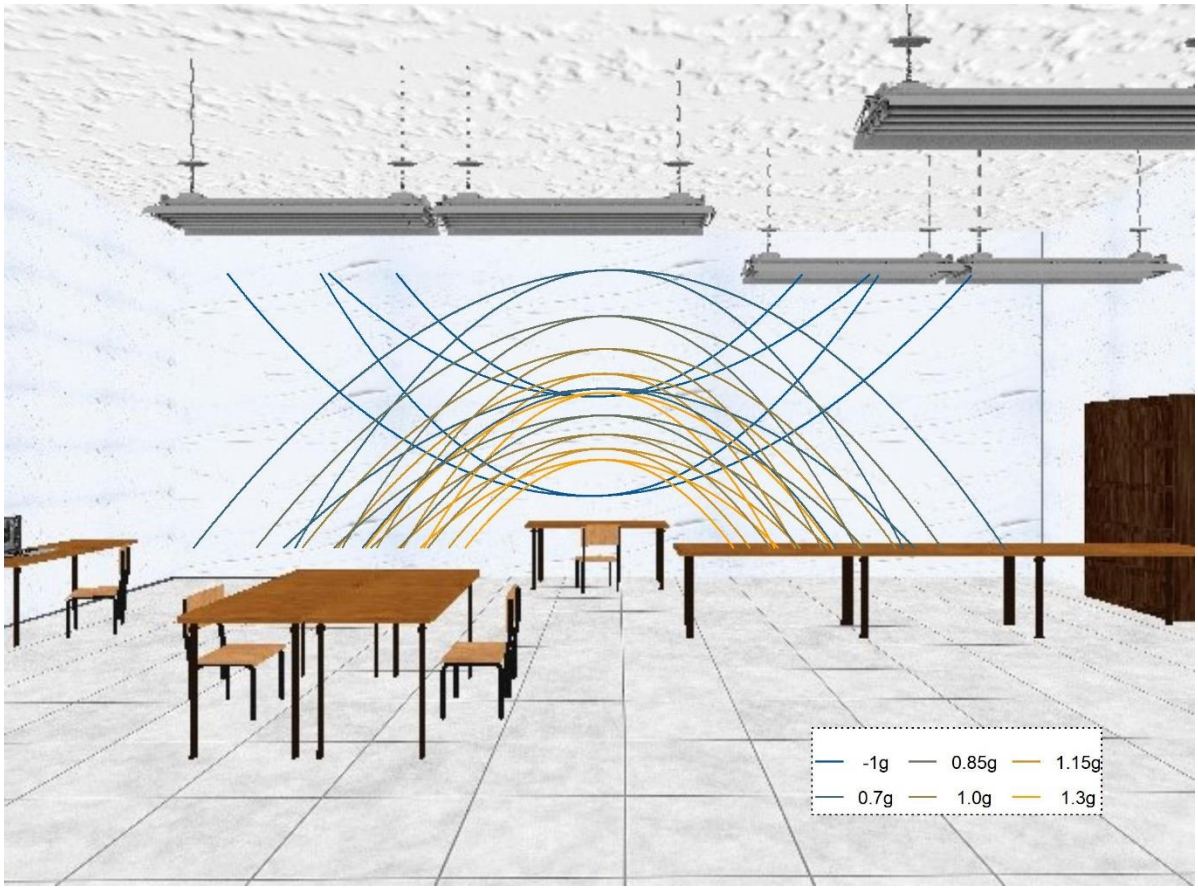

Figure 2: 2D depiction of the visual scene used as environment for stimulus presentation. The stimulus was always presented in front of the white wall and never crossed other areas (such as the lamps of tables) that could introduce low level differences in contrast etc. The lines denote the different parabolic trajectories that along which the targets travelled.

participant's inter-ocular distance. The stimuli were programmed in PsychoPy (Peirce, 2007); we added the code to our pre-registration (https://osf.io/8vg95/). The projectors introduced a delay of 0.049259 s (SD = 0.001894 s) that will be accounted for in the analysis of timing responses. Data was acquired for a different hypothesis, for which we also tracked participants eye-movements.

Procedure

Participants were first instructed to pursue the target closely with their eyes and to indicate via mouse button click when they believed the target had returned to the starting level (y = 0.5 m/y = 3.5 m). We familiarized subjects with 48 training trials (each combination of experimental variables once), in which the ball reappeared upon mouse click, thus indicating the spatial error. Then, we presented the stimuli in four blocks: 3 blocks of 320 trials each (5 gravities from 0.7g to 1.3g; 2 initial vertical velocities; 2 initial horizontal velocities; 2 occlusion conditions; 8 repetitions per combination). We furthermore tested one block of -1g/1g motion. After each block, participants could take a break. Five subjects (s1, s3, s5, s7, s9) received the 1g/-1g block as first block, while the other five subjects (s2, s4, s6, s8, s10) received it as last block.

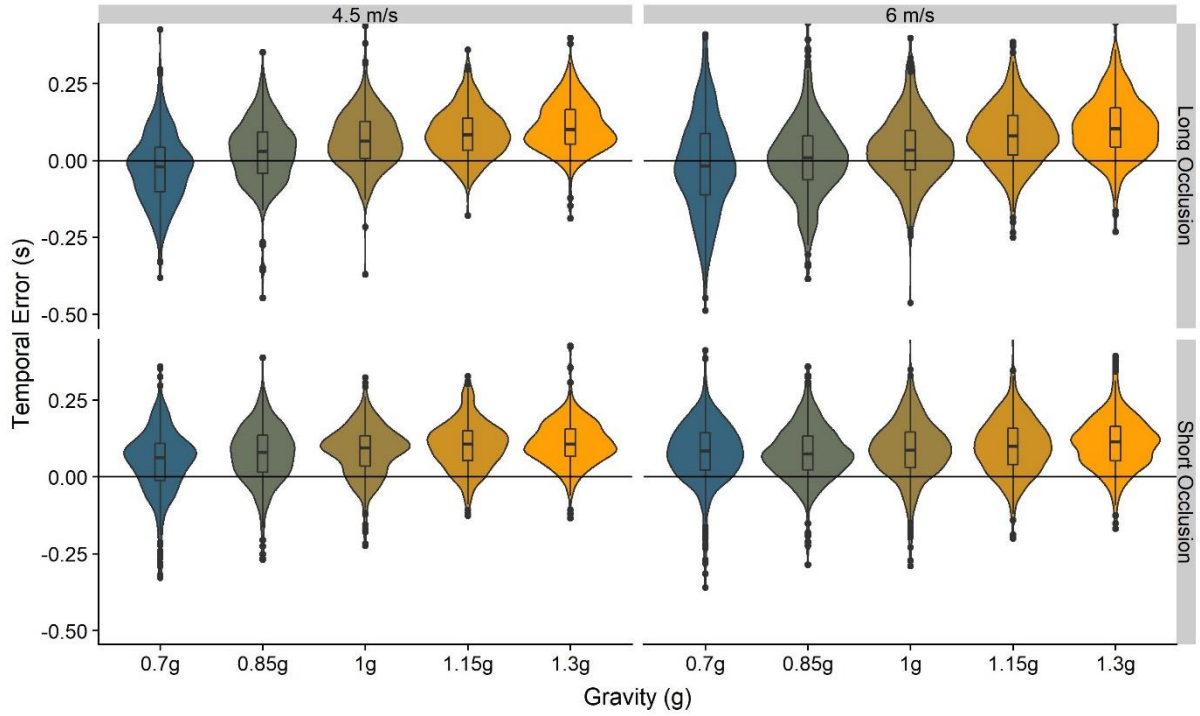

Figure 3: Temporal errors in the 0.7-1.3 g conditions. The wings of each structure indicate the distribution of responses, while the boxplot in the middle of each structure indicate the 75% percentiles and the mean per condition.

Results

While we have reported the main results of this experiment in a previous paper (Björn Jörges & López-Moliner, 2019), it is worth reiterating the results for the timing task for the conditions we are using in our

simulations. We report mean timing errors as well their standard deviations for the 0.7-1.3g trials both for the Short and the Long Occlusion conditions. Before proceeding to the analysis, we exclude all trials with an absolute error greater than 0.5 s (1091 of 13440 trials). Furthermore, we exclude all trials where subjects pressed the button before the target disappeared (26 of the remaining 12349 trials). Finally, we also excluded subject s09 from these analyses (531 of the remaining 12323 trials) because they displayed a mean temporal error (0.23 s) far above the other subjects (-0.08 to 0.1 s).

To assess biases, we fitted a Linear Mixed Model (using the lme4 package in R) where the Temporal Error is explained by Gravity as fixed effect, and intercepts per Subject as random effects. In lme4 syntax, this translates to:

$$TimingError \sim Gravity + (1\,|Subject)$$

We compare this Test Model to a Null Model, without fixed effects and only intercepts per Subject as random effects:

$$TimingError \sim (1\,|Subject)$$

An ANOVA showed that the Test Model is significantly better than the Null Model ($p < 0.001$), and the regression coefficient for Gravity is 0.022 (SE = 0.0007). That is, higher gravities are related to higher values of the temporal errors; higher gravities thus lead to too late responses, while lower gravities lead to too early responses. Figure 3: Temporal errors in the 0.7-1.3 g conditions. The wings of each structure indicate the distribution of responses, while the boxplot in the middle of each structure indicate the 75% percentiles and the mean per condition. illustrated the distributions of Temporal Errors across subjects.

To assess precision, we calculated the absolute Temporal Error for each trial with regards to the median for each condition and subject. We then fitted a Linear Mixed Model where this Precision proxy is predicted by gravity as fixed effect, and intercepts per Subject as random effects:

$$Absolute\ TimingError \sim Gravity + (1\,|Subject)$$

We compare this Test Model to a Null Model, without fixed effects and only intercepts per Subject as random effects:

$$Absolute\ TimingError \sim (1\,|Subject)$$

An ANOVA showed that the Test Model was significantly better than the Null Model ($p < 0.001$), and the regression coefficient for the fixed effect Gravity is -0.003 (SE = 0.0004). This indicates that higher gravities are related to lower variability, most likely because the interval for which the motion has to be extrapolated is shorter. Table 1 lists all mean temporal errors and the respective standard errors across participants.

		0.7g-1.3 Block					**-1g/1g Block**	
		Long Occlusion						
v_{yi}		*0.7g*	*0.85g*	*1g*	*1.15g*	*1.3g*	*-1g*	*1g*
4.5 m/s	*Mean*	-0.07	-0.02	0.02	0.04	0.06	0.09	0.04
	SD	0.11	0.10	0.09	0.08	0.08	0.11	0.09
6 m/s	*Mean*	-0.06	-0.04	-0.01	0.03	0.06	0.06	0.03
	SD	0.16	0.12	0.10	0.10	0.10	0.14	0.11

		Short Occlusion						
v_{yi}		*0.7g*	*0.85g*	*1g*	*1.15g*	*1.3g*	*-1g*	*1g*
4.5 m/s	*Mean*	0.01	0.05	0.08	0.10	0.11	0.15	0.09
	SD	0.12	0.10	0.09	0.08	0.08	0.10	0.09
6 m/s	*Mean*	0.03	0.04	0.06	0.09	0.11	0.12	0.09
	SD	0.14	0.11	0.11	0.09	0.09	0.13	0.11

Table 1: Means and standard deviations observed for the temporal errors divided by gravities and initial vertical velocities.

Interestingly, precision seems to be higher for 1g trials than for -1g trials. To test this observation statistically, we fitted a Linear Mixed Model to the -1g/1g data, where gravity as fixed effect factor and subjects as random effects predict the absolute Temporal Error as proxy for the precision:

$$Absolute\ TimingError \sim Gravity + (1\ |Subject)$$

We compare this Test Model with a Null Model where only subjects as random effects predict the absolute Temporal Error:

$$Absolute\ TimingError \sim (1\ |Subject)$$

An ANOVA showed that the Test Model was significantly better than the Null Model ($p < 0.001$), and the regression coefficient for the fixed effect factor Gravity is -0.01 (SE = 0.003), indicating that the absolute error is lower and thus the precision is higher for 1g than for -1g. On a theoretical level, this is in line with previous findings (Indovina et al., 2005) showing that the internal representation of gravity is not activated when upwards motion is presented, even when the absolute value of acceleration impacting the object is equal to the absolute value of earth gravity (9.81 m/²). The precision may thus be higher for 1g than for -1g because the internal model of gravity is utilized for 1g, but not for -1g trials.

Simulations

The physical formula for distance from initial velocity and acceleration (Equation 4) is the base for both of our simulation procedures. This reflects the assumption that humans perform the task at hand accurately – under most circumstances. This assumption is supported by our data, which show a high accuracy for the earth gravity conditions.

We furthermore neglect the air drag for these simulations and use the equation for linearly accelerated motion as an approximation.

$$d_y = \frac{g}{2} * t^2 + v_y * t \quad [4]$$

$$t_{1/2} = \frac{-v_y \pm \left({v_y}^2 - 4 * \frac{g}{2} * d_y\right)^{0.5}}{2 * \frac{g}{2}} \quad [5]$$

As evidenced by a comparison between equations (1) and (2) and equations (3) and (4), the computational complexity increases significantly if we want to accommodate air drag, while the gains in accuracy are marginal (0.02 s in the condition with the most extreme differences).

Mean of the Gravity Prior

To characterize the mean Strong Gravity Prior, we build upon our model the mean timing errors presented in our previous data (Björn Jörges & López-Moliner, 2019). Importantly, the predictions of our model matched the observed data only for the Long Occlusion condition. In the Long Occlusion condition, subjects displayed a tendency to respond slightly too late, while their responses should be centered around zero. Our ad hoc explanation of this discrepancy was that subjects were often executing a saccade when the ball returned to initial height. This saccade might have interfered with the predictions. An alternative explanation may be, however, that our subjects underestimated the target's speed at disappearance due to the so called Aubert-Fleischl phenomenon: humans estimate the speed of a target that they pursue with their eyes at about 80 % of its actual speed (Aubert, 1887; de Graaf, Wertheim, & Bles, 1991; Fleischl, 1882; Spering & Montagnini, 2011; Wertheim & Van Gelder, 1990). Our subjects were specifically instructed to follow the target with their eyes, and the eye-tracking data we collected that they generally did pursue the target. An underestimation of the velocity at disappearance could explain the tendency of subjects to respond too late in the Short Occlusion condition. For the Long Occlusion condition, on the contrary, the vertical speed at disappearance is very low and has a nearly neglectable influence on the final prediction. Setting the perceived velocity at 80 % of the presented velocity should thus yield more accurate predictions for the Short Occlusion condition, while the accuracy for the Long Occlusion condition would be largely maintained. We thus employ the same procedure laid out in (Jörges & López-Moliner, 2019), but add a coefficient of 0.8 to the perceived velocity at disappearance to account for the Aubert-Fleischl phenomenon.

We will briefly summarize the procedure and then present how this tweak affects the results of our simulations. We used the physical formula for distance from accelerated motion (Equation 4, with *d* being the height as disappearance, v_y the vertical velocity at disappearance and *g* being gravity). For our simulations, we assume that humans use an earth gravity value of 9.81 m/s² independently of the presented gravity value, as long as the display is roughly in line with a real-world scenario. We furthermore assume that we perceive the vertical velocity at disappearance at 80 % of the presented velocity. Equation 5 thus becomes

$$t_{1/2} = \frac{-v_{y,perceived} \stackrel{+}{-} \left({v_{y,perceived}}^2 - 4 * \frac{g_{earth}}{2} * d_y \right)^{0.5}}{2 * \frac{g_{earth}}{2}} \quad [5]$$

With $v_{y,perceived} = 0.8 * v_{y,presented}$ and $g_{earth} = \frac{9.81\ m}{s^2}$.

We use this formula to simulate the timing error for each trial separately without adding noise. We furthermore also simulate the responses without accounting for the Aubert-Fleischl phenomenon to compare performance for both models. Figure 4 visualizes the mean errors observed in our participants ("Obs. Error"), the mean errors when accounting for the Aubert-Fleischl phenomenon ("Sim. Error (AF)"), and the mean errors when not accounting for the Aubert-Fleischl phenomenon ("Sim. Error (No AF)").

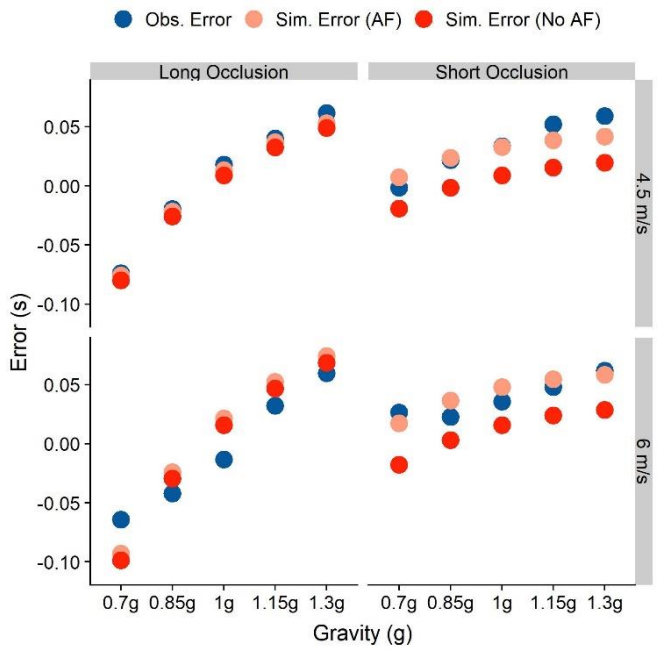

Figure 4: Mean temporal errors that we observed in our participants (blue), simulated taking the Aubert-Fleischl phenomenon into account (light red) and simulated without taking the phenomenon into account for the different conditions. The right column represents values for the Long Occlusion condition, while the left column represents the Short Occlusion condition. The upper row shows values for an initial vertical velocity of 4.5 m/s, while the lower row represents initial vertical velocities of 6 m/s.

The overall Root Mean Squared Error between AF model predictions and observed behavior is 0.014 s, and for the non-AF model predictions nearly twice as high, at 0.0244 s. Table 2 shows the error for each of the conditions. Including the AF phenomenon thus vastly improves the model's generalizability at the cost of a slight reduction in accuracy for the longest occlusion (Long Occlusion and v_y = 6 m/s).

	Long Occlusion		**Short Occlusion**	
$\mathbf{v_{yi}}$	*AF*	*No AF*	*AF*	*No AF*
4.5 m/s	0.00 s	0.006 s	0.01 s	0.03 s
6 m/s	0.025 s	0.022 s	0.009 s	0.03 s

Table 2: Root Mean Squared Errors (RMSEs) between simulated and observed mean errors for simulations including the Aubert-Fleischl phenomenon (AF) and simulations that don't (No AF). Lower values signify a better fit.

This improvement upon our previous model lends further support to the idea that the mean of a strong gravity prior is at or very close to 9.81 /s².

Standard Deviation of the Gravity Prior

The second value needed to characterize a normal distribution, which we assume the strong gravity prior to be represented as, is its standard deviation. There are two different ways to approach this problem: First, we can simulate the temporal responses of our subjects assuming different standard deviations for the gravity prior and minimize the difference between the standard deviations of the responses we observed in our subjects and the model standard deviations. In this case, we would draw the values for v_y, d_y and g_{earth} from distributions with given means and standard deviations, and compute a simulated

temporal response from these values. The mean for v_y would be the last observed velocity in y direction, corrected by a factor of 0.8 for the Aubert-Fleischl phenomenon, and the standard deviation can be computed based on Weber fractions for velocity discrimination from the literature. The mean for d_y is the distance in y direction between the point of disappearance and the reference height. The mean for g_{earth} is 9.81 m/s², and we optimize over its standard deviation to match the standard deviation observed in the subjects' temporal responses.

A second approach would be to solve equation (3) for g_{earth}, and then compute its mean and standard deviation analytically based on the means and standard deviations of t, v_y and d_y. For the addition, subtraction and multiplication of two normal distributions, there are analytic solutions to compute mean and standard deviation of the resulting distribution.

$$g_{earth} = \frac{2(d_y - v_y * t)}{t^2} \quad [6]$$

However, as evident from Equation 5, this method requires computing the standard deviation of the quotient of two distributions. To our knowledge, this is not possible in an analytical fashion and would entail simulations by itself. We will thus focus on the simulation approach.

Assumptions

For this approach, we need to make several assumptions. In the following, we will outline each and provide the rationale for the chosen values.

Use of Equation (3) – In our previous paper, we have shown that predictions based on Equation 3 fit observed temporal errors reasonably well (Björn Jörges & López-Moliner, 2019). This is particularly the case when subjects extrapolated motion for larger time frames in the Long Occlusion condition. The difference in predictions for this equation with regards to Equation (2) is at most 3 ms, and the added computational complexity does not justify the added accuracy, especially since our main concern is precision.

$\boldsymbol{v_y}$ – The velocity term in Equation 4 ($v_y * t$) refers to the part of the full distance the target moved because of its initial velocity. Our targets disappeared right after peak, therefore their initial velocity was very low. The velocity term thus contributes less to the full estimate than the gravity term, especially in the Long Occlusion condition (see also Figure 5C). Importantly, the vertical velocity component is not perceived directly. Rather, it has to be recovered from the tangential speed ($v_{tan,perceived}$) and the angle between the tangential speed vector and the vertical speed vector ($\alpha_{perceived}$) by means of the equation:

$$v_{y,perceived} = \cos(\alpha_{perceived}) * v_{tan,perceived}$$

Weber fractions for the discrimination of angular velocities reported in the literature are about 10 % (Kaiser, 1990). To calculate the standard deviation of the distribution of perceived velocities from the Weber fraction, we have to find that normal distribution where a difference of 10 % from its mode leads to a proportion of responses of 25/75 %. For a standardized normal distribution with a mean of 1, this is a standard deviation of 0.148. Note that, by using a standardized normal distribution, we assume that Weber fractions are constant across the relevant range of stimulus strengths. Figure 5C shows how predictions vary with varying variability in perceived vertical velocity: The effect is negligible for the Long Occlusion condition, while it increases response variability uniformly across gravities. Further variability is

incurred in estimating $\alpha_{perceived}$. Following (Schoups, Vogels, & Orban, 1995), the JND for orientation discrimination in untrained subjects is around 6° for oblique orientations. This corresponds to a standard deviation of 0.089.

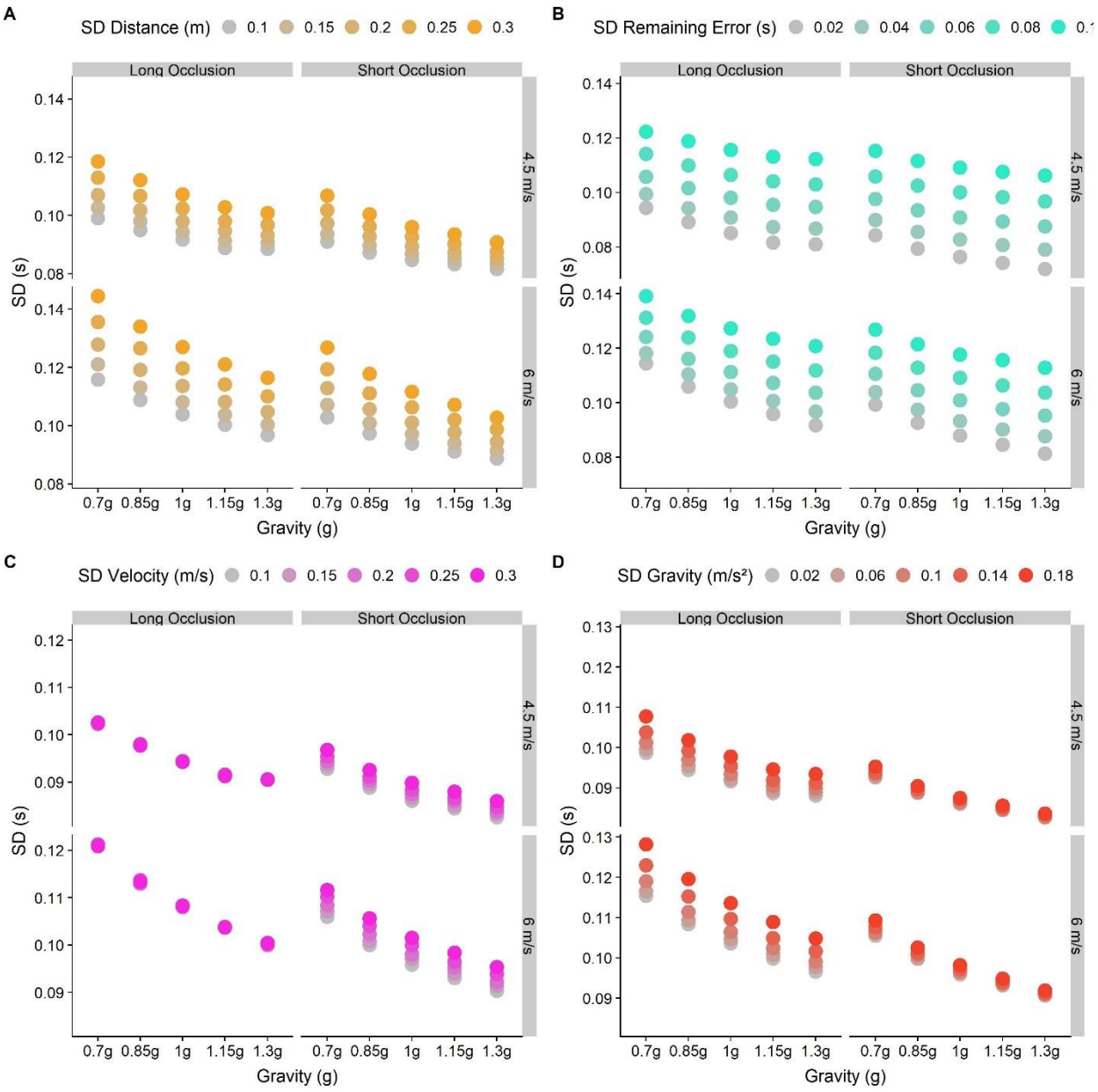

Figure 5: Predictions for different standard deviations chosen for different parameters in our model. Dots represent the standard deviation for each gravity (0.7g-1.3g), divided by Occlusion category (Long and Short) and initial vertical velocities (4.5 and 6 m/s). The color gradient indicates different values of the (standardized) standard deviation for the perceived distance, the perceived velocity, the represented gravity and the remaining error. The baseline values are 0.148 for distance and velocity, 0.1 for gravity and 0.05 for the remaining (motor) error. A. Predictions for five standardized standard deviations for the perceived distance (0.1-0.3 m). B. Predictions for five standard deviations for the remaining (motor) error (0.02-0.1 s), modelled as independent of and constant across initial velocities, gravities and occlusion conditions. C. Predictions for five different standardized standard deviations for the last perceived velocity (0.1-0.3 m/s). D. Predictions for five different standardized standard deviations for the represented gravity (0.02-0.18 m/s²).

Furthermore, we need to account for the Aubert-Fleischl phenomenon, which consists in an underestimation of the velocity of a moving target during smooth pursuit (Aubert, 1887; de Graaf et al., 1991; Fleischl, 1882; Spering & Montagnini, 2011; Wertheim & Van Gelder, 1990). While this effect should in principle be partially offset by improved predictions for motion coherent with earth gravity – an empirical question that has, to our knowledge, not been addressed so far –, our simulations show that a Aubert-Fleischl correction factor of 0.8 yields an excellent fit for the observed mean errors. We thus proceed with a value of 0.8 also for the simulations concerning the standard deviation.

$\boldsymbol{d_y}$ – For the distance term (d_y), we choose the stimulus value as mean distance, as we don't expect any biases. In terms of precision, Weber fractions of 3 % to 5 % are observed for distance estimates in the front parallel plane (Norman, Todd, Perotti, & Tittle, 1996). However, since subjects have to estimate the distance not between two well defined points, but rather the height above the simulated table, the precision of these estimates is likely lower than reported for the above task. We thus work with a Weber fraction of twice the reported value (10 %). Using the above method, we determine that the standard deviation for this value is 0.148. Figure 5A shows how predictions vary with variability in perceived distance: There is a slight logarithmic pattern, where response variability added by higher variability in perceived distance increases with decreasing gravity.

t – The response time t is measured directly in our task, both in mean and variability.

Remaining Variability – For our simulations, we rely on accounting for every source of variability in the responses. One source of error beyond perceiving and representing $\mathbf{g}$, $\boldsymbol{v_y}$ and $\boldsymbol{d_y}$ is the motor response. Motor responses are likely to vary strongly between tasks, for which reason variability reported in the literature is of limited use. To estimate the error introduced by these further factors, we thus take advantage of previous results indicating that the gravity model is not activated for upside-down motion (Indovina et al., 2005), a hypothesis which is also supported by our data.

Under this assumption, we can use the responses for the inverted gravity condition to estimate the errors introduced by motor variability. An inactivation of the gravity prior would mean that the gravity acting upon the object should be represented with the same precision as arbitrary gravities. We previously found Weber fractions of between 13 % and beyond 30% for arbitrary gravities (Björn Jörges, Hagenfeld, & López-Moliner, 2018), which is in line with those found for linear accelerations (Werkhoven, Snippe, & Alexander, 1992). We thus proceed with a value of 20 %, which corresponds to a normalized standard deviation of 0.295 (see procedure above).

There are further constraints: First, the motor variability should be lower than the overall variabilities observed for each condition (the minimum is just over 0.08 s for the short occlusion condition with 1.3g and an initial vertical velocity of 4.5 m/s). Second, the motor variability should be equal across conditions and be independent of gravity, initial velocity and Occlusion category (see Figure 5B).

We put these values for $\mathbf{g}$, $\boldsymbol{v_y}$ and $\boldsymbol{d_y}$ into Equation 4 to stimulate the temporal responses for each trial 1000 times. We minimize the Root Mean Square Errors (RMSE) between the standard deviations of the simulated timing error and the observed timing errors. After visualizing a relevant range of candidate values for the standard deviation of the remaining errors (see Figure 6), we use the optim() function implemented in R with a lower bound of 0.01 s and an upper bound of 0.06 s to find the best fit for the observed data. We found the best fit for a standard deviation of 0.03 s, with an RMSE of 0.015 s.

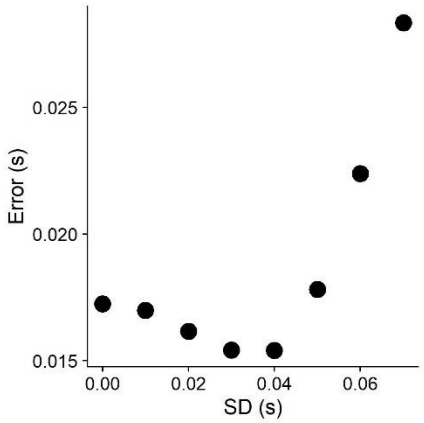

Figure 6: Root mean square errors (RMSE) between the standard deviation of timing errors simulated based on different motor errors (between 0.00 and 0.07 s) and the standard deviation of observed timing errors.

The Standard Deviation of the Gravity Prior

We then proceed to apply these values to simulate data sets based on the above assumptions, get the standard deviations for the timing error and compare them to standard deviations of the observed timing errors (Method 1). We restrict this comparison to the 0.7g/0.85g/1g/1.15/1.3g condition, as we expect the gravity model not to be activated for inverted gravitational motion. For a discussion of factors impacting the performance of the model for short occlusions, see (Jörges et al., 2018). We first simulate a range of sensible standard deviations (from 0 m/s^2, corresponding to an impossibly precise representation, to 0.28 m/s^2, corresponding to a quite imprecise representation with limited impact on the final percept, in steps of 0.03 m/s^2) to determine the lower and upper bounds of the optimization interval (see Figure 7); Figure 5D furthermore highlights how changes in the simulated variability of the represented gravity changes response variability.

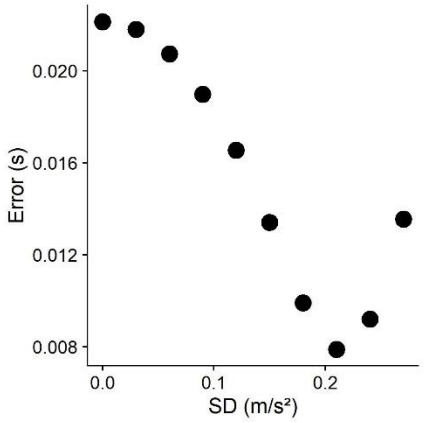

*Figure 7: Root mean square errors (RMSE) between the standard deviation of timing errors simulated based on different standard deviations of the gravity prior between 0.15 and 0.25*9.81 m/s^2 and the standard deviation of observed timing errors.*

We find the errors to be lowest around 0.21 m/s^2, and choose thus 0.16 m/s^2 as the lower bound and 0.26 m/s^2 as the upper bound. We then search for that standard deviation that minimizes the error

between simulated and observed timing errors, using the optim() function implemented in R (R Core Team, 2017). For each iteration, we simulate 1000 data sets and minimize the Root Mean Square Error (RMSE) between the standard deviations of simulated and observed timing errors across these 1000 data sets. The R code we used for these simulations can be found on GitHub (https://github.com/b-jorges/SD-of-Gravity-Prior), including extensive annotations. We found a normalized standard deviation of 0.217 m/s² for the gravity prior, which corresponds to a standard deviation of about 2.13 m/s² for a mean of 9.81 m/s² and a Weber fraction of 14.6 %. The RMSE is 0.008 s. In Figure 8, we illustrate how the simulated standard deviations relate to the observed ones. The light red dots correspond to this method ("Simulated (Method1)"); as evident from the figure, the fits are better for the short occlusion condition, while the SDs are generally underestimated for the Long Occlusion condition.

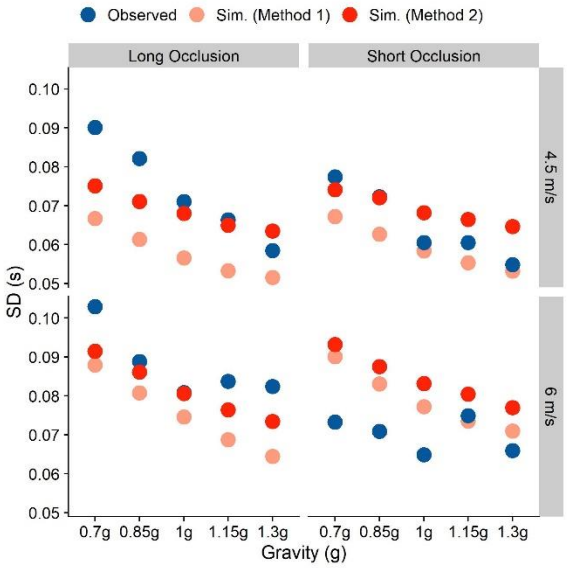

Figure 8: Observed and Simulated Standard Deviations separated by Occlusion Condition, initial vertical velocity and presented gravity. Blue indicates the observed standard deviations across subjects, while the standard deviations simulated through the two-step process (Method 1) are coded light red and the standard deviations simulated through the two-parameter fit (Method 2) are coded solid red.

As there is some reason to believe that the gravity prior is not completely inactive in upwards motion, which may bias to above method to overestimate the standard deviation of the gravity prior, we furthermore conducted simulations where both the motor variability and the strong gravity prior are fitted to the data (Method 2). To this end, we use the optimize() function implemented in R which uses the Nelder and Mead method (Nelder & Mead, 1965) to determine those values for the motor standard deviation and the standard deviation of the gravity prior that yield the smallest errors between simulated and observed variability. This is suitable, as variability in the gravity prior and motor variability affect the final variability differentially (see Figure 5): a higher motor variability leads to uniformly higher standard deviations for the observed error, while a higher gravity variability affects longer trajectories (Long Occlusion, higher initial vertical velocity and lower gravities) more strongly than shorter ones. Based on above results, we chose 0.04 and 0.2 as starting parameters, but did not limit the parameter space. This method allots variability in slightly different proportions: the standard deviation for the motor error is 0.05 s and the standardized standard deviation of the gravity prior is 0.182 m/s² (which corresponds to a non-standardized standard deviation of 1.78 m/s² and a Weber fraction of 12.2 %), with an RMSE of

0.005 s. This is considerably lower than the RMSE of 0.008 s found with the Method 1. However, it is worth noting that fitting both parameters to the data makes this method more susceptible to overfitting. The simulated standard deviations for these conditions are depicted in solid red in the Figure 8 ("Simulated (Method 2)"): The fits are much better for the long occlusions, at the cost of a slight overestimation of the variability for the short occlusions.

Discussion

Humans assume in many tasks and circumstances that objects in their environment are affected by earth gravity. It has thus been suggested that we maintain a representation of this value, which we then recruit to predict the behavior of objects in our environment. We recently interpreted this representation as a Strong Prior in a Bayesian framework (Björn Jörges & López-Moliner, 2017). A "Strong Prior" is a prior with a reliability so high that it overrules any sensory input represented in the likelihood. Based on data from timing task (previously reported in Jörges & López-Moliner, 2019), we make an attempt at determining the standard deviation of a hypothetical Strong Earth Gravity Prior. Our general approach is to account for other sources of perceptuo-motor variability in the task based on thresholds reported in the literature, and attributing the remaining variability to the Gravity Prior. Based on this approach, we find a standard deviation of 2.13 m/s² (Method 1) or 1.78 m/s² (Method 2), for a prior with a mean of 9.81 m/s², which corresponds – mathematically – to a Weber fraction of 14.6 % or 12.2 %, respectively. This is considerably lower than Weber fractions generally observed for acceleration discrimination, but above Weber fractions for the discrimination of constant speeds (McKee, 1981).

Interestingly, when we simulated the timing errors with a fixed value of 9.81 m/s² (i. e. in a non-Bayesian framework where the value of earth gravity is not represented as a distribution, but rather a value set at 1g; see Jörges & López-Moliner, 2019 and also above), we found that our results fit the observed timing error quite nicely for each gravity value. That is, the observed gravity (corresponding to the Likelihood) had no discernable influence on the final percept (Posterior). However, in a Bayesian framework, this is only possible if the Likelihood is extremely shallow and the Prior is extremely precise. A Weber fraction of about 30 % for the likelihood (which we assume for acceleration discrimination), and a Weber fraction of 14.6 % or 12.2 %. for the prior (as modelled) would not result in discarding the likelihood completely (see also Figure 1; even for a strong prior and a rather shallow likelihood, the likelihood attracts the posterior to some extent). Our results thus reveal a mismatch between the means observed in our experiment, the modelled standard deviation and a Bayesian explanation.

We see two possible ways to explain this mismatch. Firstly, our observed standard deviation for the gravity prior could be an upper bound. Our method relies on identifying all sources of variability and allotting variability in the response accordingly. Since we did not measure our participants' Weber fractions for velocity and distance discriminations individually, but rather used averages reported in the literature for somewhat different tasks, this may have distorted how much variability perceived distances and velocity at disappearance introduced in the response. Furthermore, when estimating the variability introduced in the motor response, we part from the premise that the internal model of gravity is not activated at all for -1g motion. However, we observe a bias to respond too late in this condition, suggesting that humans expect objects to accelerate less when moving upwards. This could be taken as evidence that the internal model of gravity is still activated to some extent. In this case, we would need to allot more variability to the motor error, which in turn would lead to a lower standard deviation for the gravity prior. However,

this pattern in our data is also consistent with humans taking arbitrary accelerations into account insufficiently in perceptuo-motor tasks, which has been reported repeatedly for tasks where the gravity prior is highly unlikely to be recruited (Benguigui, Ripoll, & Broderick, 2003; Bennett & Benguigui, 2013; Brenner et al., 2016; Werkhoven et al., 1992). The values of 14.6 % or 12.2 % obtained above may thus be an upper bound for the standard deviation of the Earth Gravity Prior.

A second possibility is that prior knowledge and online perceptual input are combined in a non-Bayesian fashion (and we should thus avoid the terminology "Prior", "Likelihood" and "Posterior"), where the mean of the final percept is set according to an acceleration of 9.81 m/s², while its standard deviation is determined by a (not necessarily Bayesian) combination of prior knowledge and online sensory information.

Conclusion

In this paper, we build upon a simple model for coincidence timing of gravitational motion brought forward in (Björn Jörges & López-Moliner, 2019). By accounting for the Aubert-Fleischl phenomenon, we extend the domain of our model to also include shorter extrapolation intervals. Furthermore, we propose a procedure to determine the standard deviation of a potential gravity prior, and apply it to pre-existing data from a timing task. Standard deviations of 2.13 m/s² or 1.78 m/s² (depending on the method) explains the behavior observed in our task best. However, considering the literature we would expect an even lower standard deviation, as a Prior with a mean of 9.81 m/s² and standard deviations of 2.13 m/s² or 1.78 m/s² should not attract the Posterior as strongly as has been commonly observed. We thus believe that we are not able to fully disentangle different sources of noise in our data; the value we find for the standard deviation of the earth gravity prior is thus more likely an upper bound, and follow-up experiments may find lower values.

Author Contributions and Notes

BJ conducted the simulations and wrote the paper. BJ and JLM established the research question in a joint effort. JLM provided advice at every step of the project.

The authors declare no conflict of interest.

Acknowledgments

Funding was provided by the Catalan government (2017SGR-48) and the project ref. PSI2017-83493-R from AEI/Feder, UE. The first author (BJ) was supported by the Canadian Space Agency (CSA).

References

Aubert, H. (1887). Die Bewegungsempfindung. *Pflüger, Archiv Für Die Gesammte Physiologie Des Menschen Und Der Thiere*, *40*(1), 459–480. https://doi.org/10.1007/BF01612710

Benguigui, N., Ripoll, H., & Broderick, M. P. (2003). Time-to-contact estimation of accelerated stimuli is based on first-order information. *Journal of Experimental Psychology. Human Perception and*

Performance, *29*(6), 1083–1101. https://doi.org/10.1037/0096-1523.29.6.1083

Bennett, S. J., & Benguigui, N. (2013). Is Acceleration Used for Ocular Pursuit and Spatial Estimation during Prediction Motion? *PLoS ONE*, *8*(5). https://doi.org/10.1371/journal.pone.0063382

Brenner, E., Rodriguez, I. A., Muñoz, V. E., Schootemeijer, S., Mahieu, Y., Veerkamp, K., … Smeets, J. B. J. (2016). How can people be so good at intercepting accelerating objects if they are so poor at visually judging acceleration? *I-Perception*, *7*(1), 1–13. https://doi.org/10.1177/2041669515624317

Ceccarelli, F., La Scaleia, B., Russo, M., Cesqui, B., Gravano, S., Mezzetti, M., … Zago, M. (2018). Rolling motion along an incline: Visual sensitivity to the relation between acceleration and slope. *Frontiers in Neuroscience*, *12*(JUN), 1–22. https://doi.org/10.3389/fnins.2018.00406

de Graaf, B., Wertheim, A. H., & Bles, W. (1991). The Aubert-Fleischl paradox does appear in visually induced self-motion. *Vision Research*, *31*(5), 845–849. https://doi.org/10.1016/0042-6989(91)90151-T

Dichgans, J., Wist, E., Diener, H. C., & Brandt, T. (1975). The Aubert-Fleischl phenomenon: A temporal frequency effect on perceived velocity in afferent motion perception. *Experimental Brain Research*, *23*(5), 529–533. https://doi.org/10.1007/BF00234920

Fleischl, V. (1882). Physiologisch-optische Notizen. *Sitzungsberichte Der Akademie Der Wissenschaften Wien*, (3), 7–25.

Indovina, I., Maffei, V., Bosco, G., Zago, M., Macaluso, E., & Lacquaniti, F. (2005). Representation of visual gravitational motion in the human vestibular cortex. *Science (New York, N.Y.)*, *308*(April), 416–419. https://doi.org/10.1126/science.1107961

Jörges, B., & López-Moliner, J. (2019). Earth-Gravity Congruent Motion Facilitates Ocular Control for Pursuit of Parabolic Trajectories. *Scientific Reports*, *9*(1). https://doi.org/10.1038/s41598-019-50512-6

Jörges, Björn, Hagenfeld, L., & López-Moliner, J. (2018). The use of visual cues in gravity judgements on parabolic motion. *Vision Research*, *149*, 47–58. https://doi.org/10.1016/J.VISRES.2018.06.002

Jörges, Björn, & López-Moliner, J. (2017). Gravity as a Strong Prior: Implications for Perception and Action. *Frontiers in Human Neuroscience*, *11*(203). https://doi.org/10.3389/fnhum.2017.00203

Jörges, Björn, & López-Moliner, J. (2019). Earth-Gravity Congruent Motion Facilitates Ocular Control for Pursuit of Parabolic Trajectories. *Scientific Reports*, *9*(1), 1–13. https://doi.org/10.1038/s41598-019-50512-6

Kaiser, M. K. (1990). Angular velocity discrimination. *Perception & Psychophysics*, *47*(2), 149–156. https://doi.org/10.3758/BF03205979

La Scaleia, B., Zago, M., Moscatelli, A., Lacquaniti, F., & Viviani, P. (2014). Implied dynamics biases the visual perception of velocity. *PLoS ONE*, *9*(3). https://doi.org/10.1371/journal.pone.0093020

Lacquaniti, F., Bosco, G., Indovina, I., La Scaleia, B., Maffei, V., Moscatelli, A., & Zago, M. (2013). Visual gravitational motion and the vestibular system in humans. *Frontiers in Integrative Neuroscience*, *7*(December), 101. https://doi.org/10.3389/fnint.2013.00101

Maffei, V., Indovina, I., Macaluso, E., Ivanenko, Y. P., Orban, G. A., & Lacquaniti, F. (2015). Visual gravity cues in the interpretation of biological movements: Neural correlates in humans. *NeuroImage*,

104(October 2014), 221–230. https://doi.org/10.1016/j.neuroimage.2014.10.006

McIntyre, J., Zago, M., & Berthoz, A. (2001). Does the Brain Model Newton's Laws. *Nature Neuroscience*, *12*(17), 109–110. https://doi.org/10.1097/00001756-200112040-00004

McKee, S. P. (1981). A local mechanism for differential velocity detection. *Vision Research*, *21*(4), 491–500. https://doi.org/10.1016/0042-6989(81)90095-X

Monache, S. D., Lacquaniti, F., & Bosco, G. (2019). Ocular tracking of occluded ballistic trajectories: Effects of visual context and of target law of motion. *Journal of Vision*, *19*(4), 1–21. https://doi.org/10.1167/19.4.13

Moscatelli, A., & Lacquaniti, F. (2011). The weight of time: Gravitational force enhances discrimination of visual motion duration. *Journal of Vision*, *11*(4), 1–17. https://doi.org/10.1167/11.4.1

Nelder, J. A., & Mead, R. (1965). A Simplex Method for Function Minimization. *The Computer Journal*, *7*(4), 308–313. https://doi.org/10.1093/comjnl/7.4.308

Norman, J. F., Todd, J. T., Perotti, V. J., & Tittle, J. S. (1996). The Visual Perception of Three-Dimensional Length. *Journal of Experimental Psychology: Human Perception and Performance*, *22*(1), 173–186. https://doi.org/10.1037/0096-1523.22.1.173

Peirce, J. W. (2007). PsychoPy—Psychophysics software in Python. *Journal of Neuroscience Methods*, *162*(1–2), 8–13. https://doi.org/10.1016/J.JNEUMETH.2006.11.017

R Core Team. (2017). *A Language and Environment for Statistical Computing. R Foundation for Statistical Computing,*. Retrieved from http://www.r-project.org/.

Schoups, A. A., Vogels, R., & Orban, G. A. (1995). Human perceptual learning in identifying the oblique orientation: retinotopy, orientation specificity and monocularity. *The Journal of Physiology*, *483*(3), 797–810. https://doi.org/10.1113/jphysiol.1995.sp020623

Senot, P., Zago, M., Le Seac'h, a., Zaoui, M., Berthoz, a., Lacquaniti, F., & McIntyre, J. (2012). When Up Is Down in 0g: How Gravity Sensing Affects the Timing of Interceptive Actions. *Journal of Neuroscience*, *32*(6), 1969–1973. https://doi.org/10.1523/JNEUROSCI.3886-11.2012

Spering, M., & Montagnini, A. (2011). Do we track what we see? Common versus independent processing for motion perception and smooth pursuit eye movements: A review. *Vision Research*, *51*(8), 836–852. https://doi.org/10.1016/j.visres.2010.10.017

Werkhoven, P., Snippe, H. P., & Alexander, T. (1992). Visual processing of optic acceleration. *Vision Research*, *32*(12), 2313–2329. https://doi.org/10.1016/0042-6989(92)90095-Z

Wertheim, A. H., & Van Gelder, P. (1990). An acceleration illusion caused by underestimation of stimulus velocity during pursuit eye movements: Aubert-Fleischl revisited. *Perception*, *19*(4), 471–482. https://doi.org/10.1068/p190471

Zago, M., La Scaleia, B., Miller, W. L., & Lacquaniti, F. (2011). Coherence of structural visual cues and pictorial gravity paves the way for interceptive actions. *Journal of Vision*, *11*(10), 1–10. https://doi.org/10.1167/11.10.13.Introduction

Zago, M., McIntyre, J., Senot, P., & Lacquaniti, F. (2008). Internal models and prediction of visual gravitational motion. *Vision Research*, *48*(14), 1532–1538. https://doi.org/10.1016/j.visres.2008.04.005